Tunnelling and Underground Space Technology 41 (2014) 193–205

Contents lists available at ScienceDirect

Tunnelling and Underground Space Technology

journal homepage: www.elsevier.com/locate/tust

Model test study on effective ratio of segment transverse bending rigidity of shield tunnel

Ye Fei *, Gou Chang-fei, Sun Hai-dong, Liu Yan-peng, Xia Yong-xu, Zhou Zhuo

Chang'an University, Shaanxi Provincial Major Laboratory for Highway Bridge & Tunnel, Xi'an 710064, China

ARTICLE INFO

Article history:
Received 13 August 2012
Received in revised form 26 December 2013
Accepted 30 December 2013
Available online 29 January 2014

Keywords:
Shield tunnel
Bending rigidity efficiency
Model test
Straight-jointed assembly
Stagger-jointed assembly

ABSTRACT

The effective ratio of the transverse bending rigidity has an important influence on internal force of segmental ring, and that is an important parameter in shield segment design with average uniform rigidity ring. Based on tensile tests and similarity theory (at the joint area, similarity relation is achieved from the model tunnel which has the same rigidity ratios with the prototype tunnel), three kinds of segmental ring test models made of PMMA (to simulate segment) and aluminum welding wire (to simulate bolt) are used to carry out the model test, which include straight-jointed ring, stagger-jointed ring and uniform ring. Through changing the number of spring gaskets, the different bolt pre-tightening forces of straight-jointed and stagger-jointed ring are obtained. The multi-stage loading test on straight-jointed ring, stagger-jointed ring and uniform ring under different bolt pre-tightening forces are carried out with a homemade loading device. The variation values of horizontal and vertical diameter of straight-jointed and stagger-jointed ring are compared respectively, and then it is concluded that the range of the effective ratio of the transverse bending rigidity value is between 0.09 and 0.23 under straight-jointed condition, 0.30 and 0.80 under stagger-jointed condition. The contrast analysis on the effective ratio of the transverse bending rigidity values under different load levels with different bolt pre-tightening forces and different assembly modes shows that value of the stagger-jointed segmental ring is obviously lager than that of the straight-jointed segmental ring, and that difference decrease gradually with the load increasing.

1. Introduction

The shield-driven tunneling method is widely adopted for the construction of city subway tunnel, municipal tunnel and underwater tunnel, due to its flexibility, cost effectiveness and the minimum impact on surrounding soil. As the lining of a shield-driven tunnel is not a continuous ring structure due to the existence of joints, the effect of the joints on internal forces and displacements should be taken into consideration in the design of tunnel lining. Shield tunnel segments are often articulated or coupled at the longitudinal and circumferential joints. Therefore, not only the characteristics of the concrete segments influence the structure but also the mechanical and geometrical characteristics of the joints strongly affect the structural behavior of the tunnel lining (Klappers et al., 2006). Hudoba (1997) had taken into consideration the effects of the segment ring joints in his study. Gruebl (2012) pointed out that the determination of loads during ring erection, advance of the TBM, earth pressure and bedding of the articulated ring is difficult, and the ring model and the design input values must be studied carefully according to the parameters of the surrounding soil. Through diagrams for the hoop forces, bending moments and radial displacements, Duddeck and Erdmann (1982) illustrated the differences in the design values evaluated for three different models – the continuum model, the Muir Wood design model and the bedded beam model without bedding at the crown region. With respect to the actual design methods for the shield tunnel linings, the loads acting on the tunnel linings should be firstly determined, and then the material and the cross-sectional dimensions of the segments are determined by structural analysis. It is, therefore, very significant to choose an appropriate design model (or method) for the determination of the internal forces in each part of a segment and its interaction under different loads. There are a number of design models suggested by ITA (ITA, 2000). Lee et al. (2001) classified all tunnel lining design methods into four major types: (a) empirical design methods based on past tunneling practices; (b) design methods based on in-situ measurement and laboratory testing; (c) circular ring in elastic foundation method; and (d) continuum mechanics models including analytical methods and numerical methods.

As for the shield tunnel linings, the segment structure was often been separated into two plane problems along transverse and

* Corresponding author. Address: School of Highway, Chang'an University, Nan Er Huan Zhong Duan, Xi'an 710064, Shaanxi, China. Tel.: +86 29 82338926; fax: +86 29 82334838.
E-mail address: xianyefei@sohu.com (F. Ye).

0886-7798/$ - see front matter © 2014 Elsevier Ltd. All rights reserved.
http://dx.doi.org/10.1016/j.tust.2013.12.011

longitudinal direction in design or study process, although it was a 3D structure apparently (Liao, 2002; Liao et al., 2008). In transverse direction, the segmental circular lining system is usually designed in the plane strain condition (ITA, 2000; Bakker, 2003; BTS, 2004; Huang et al., 2012), and the third method "circular ring in elastic foundation method" in aforementioned models is by far most commonly adopted for design purposes. There are a number of proposed structure models so far in accordance with the treatment of the joints of segments, the corresponding structural models are shown in Fig. 1 (Koyama, 2000).

(1) Uniform rigidity ring, the circumferential joint is assumed to have the same rigidity as that of the segment, the moment for the design of joint is overestimated and that occurring at the segment cannot be calculated correctly. Therefore, it is difficult to compute the bending moment at the joint area.
(2) Average uniform rigidity ring, an average uniform rigidity ring model was proposed in order to make up for the faults of the uniform rigidity ring model. Two factors (the effective ratio of the transverse bending rigidity η and the additional rate of bending moment ξ) were applied to this model. The decrease of the bending stiffness at the joint is considered as the decrease of the ring, accordingly, the equivalent stiffness of the segmental ling ring is ηEI ($\eta \leqslant 1$). Under the condition of stagger-jointed assembly, $(1+\xi)M_0$ (M_0 is the moment in tunnel lining without joint) is adopted as the main moment for the segment and $(1-\xi)M_0$ is taken as the design moment of the joint (shown in Fig. 2, Peck et al., 1972; Muir Wood, 1975; JSCE, 1977; Koyama, 2003).
(3) Multi-hinge ring, the rigidity of the joint is ignored, and the joins are assumed as hinges. As a non-static structure, the lining ring can turn to a static structure only with surrounding pressures including soil resistance around the lining structure. Therefore, the surrounding pressures condition and soil resistance has an important influence on stress, deformation and performance of the segmental lining ring, and this model is only suitable for hard stratum (Tang, 1988).
(4) Beam-spring model, the segments are modeled as beams and the joints are simulated by the rotation of springs, and their rigidities are expressed by the constants of the springs concerning the bending moments. The model can be subdivided into beam-spring (I) and (II) according to whether the relative displacement between the two neighboring rings in the longitudinal direction is to be considered or not (Zhu and Tao, 1998; Koyama, 2003; Hu et al., 2009).

The average uniform rigidity ring model is often used in today's segment structure design of shield tunnel, in which the value of the effective ratio of the transverse bending rigidity is crucial, as low value may lead to unnecessary waste in the segmental lining design process, while high value may result in hidden trouble of insufficient bearing capacity of the segmental lining. Furthermore, the value of the effective ratio of the transverse bending rigidity has an important influence on internal force of segmental ring, and the rationality of that directly determines whether the stress and deformation behavior of the tunnel lining is truly displayed by the average uniform rigidity ring model (Koyama and Nishimura, 1998). Presently, the study on the effective ratio of the transverse bending rigidity concentrates on the value and influence factors, with the research methods of theoretical analysis and model test. Muir Wood (1975) proposed experiential formula for calculating the effective ratio of the transverse bending rigidity considering the effects of segment number and joint stiffness. Based on the hypothesis of ellipsoid deformation, Liu and Hou (1991) deduced the calculation method of stiffness reduction coefficient of segment ring with joints in contrast to continuous ring. Lee and Ge (2001) calculated the effective ratio of the transverse bending rigidity of average uniform rigidity ring method with the multi-hinge ring model, and proposed the fitting formula of the effective ratio of the transverse bending rigidity and various parameters (including the radius of tunnel, lining thickness, strata resistance coefficient, and joints stiffness ratio) under the condition of straight-jointed assembly. Zhong et al. (2003) obtained the value of the effective ratio of the transverse bending rigidity through calculating the maximum horizontal displacement with average uniform rigidity ring and beam-spring model separately. Therefore, they put forward the simple determination method of the effective ratio of the transverse bending rigidity η, after summarizing the bending stiffness ratio λ between bending rigidities of segments and that of joints of Chinese subway tunnels. They considered that segment assembly mode, such as the straight-jointed assembly and stagger-jointed assembly, has a small influence on transverse bending rigidity of segmental ling structure. Taking Shanghai subway tunnel as the research object, Xu (2005) and Huang et al. (2006a) analyzed the value of the

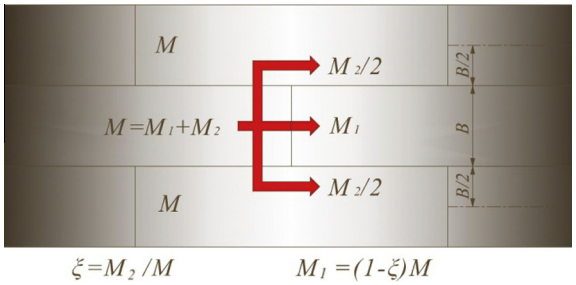

Fig. 2. Concept of the additional rate of bending rigidity (Koyama, 2003).

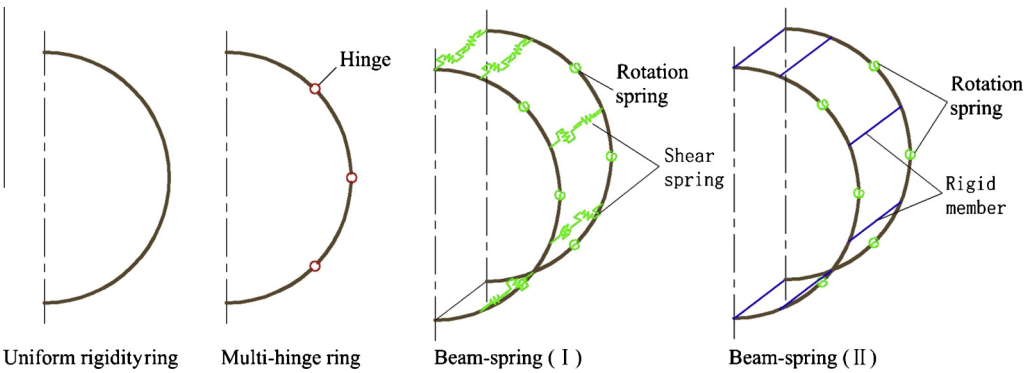

Fig. 1. Structural models of the segment ring (Koyama, 2000).

effective ratio of the transverse bending rigidity by the means of laboratory model tests. They suggested the value of η equals 0.67 in straight-jointed assembly condition and 0.75 in stagger-jointed assembly condition. Huang et al. (2006b) analyzed the influence of joint stiffness on the effective ratio of the transverse bending rigidity η and the additional rate of bending moment ξ, and then, proposed the calculating method of the effective ratio of the transverse bending rigidity with circumferential and radial relative stiffness. Huang et al. (2010) took the largest diameter tunnel in the world, Shanghai Yangtze River tunnel, as the research background, used a full scale horizontal integral ring of lining structure to carry on the loading experiment, and got the conclusion that the shape and measured deformation value of the middle ring closely met calculated value when the effective ratio of the transverse bending rigidity η equals 0.8. On the basis of segmental lining structure prototype tests of big cross section shield tunnel (including Nanjing Yangtze River Shield Tunnel and Guangzhou Zhujiang River Shiziyang Shield Tunnel) and the analysis on the influence factors, Feng et al. (2011) proposed calculating method of the effective ratio of the transverse bending rigidity, and obtained the variation pattern of η and ξ with the load conditions. The recommended value of η was 0.8, and ξ was 0.3 in Japanese standards (Japan Society of Civil Engineers, Zhu translates, 2001), and the η value used in the structure design of Trans-Tokyo Bay Highway shield tunnel was 0.8 (Uchida, 1992). Japanese scholars (Kashima et al., 1996) developed the DPLEX shield method and carried out the prototype loading tests on segmental lining structure, and the test result showed that the value of η equal to 0.8 was reasonable.

Anyway, the segmental ring is erected in the shielded TBM and during the advance, the rams act on the ring; therefore, the ring never can be seen independent from the TBM (Gruebl, 2006). The interaction between machine, thruster configuration and geometry of the segments will influence the kinematics of erector and segments. The German Committee for Underground Construction (DAUB) has published recommendations for the structural analysis of shield machines in November 2005 (Grübl and Thewes, 2006). In fact, DAUB also published recommendations of "Concrete Linings for Tunnel built by underground Construction" (DAUB, 2001), in which the process of segments design, production and installing was generally introduced. Many researchers have tried to analyze the shield tunnel with numerical method. Kasper and Meschke (2004) proposed a three-dimensional finite element model for shield tunneling in soft, water saturated soil, which taken into account all relevant components and realistically models the step-by-step construction process. They also evaluated the influence of the face and grouting pressure and the TBM design with respect to various important tunneling design criteria such as the surface settlements, the shield movement and the loading of the tunnel lining (Kasper and Meschke, 2006). Ding et al. (2004) proposed a two-dimensional finite element method for analyzing shield tunnels during construction.

In this paper, the mechanical behaviors of segmental ring and the η value are studied by laboratory structural model testing on the basis of the previous research: (1) According to similarity theory, three kinds of segmental ring test models, including straight-jointed ring, stagger-jointed ring and uniform ring, are used to carry out the model test, which are made of PMMA (to simulate segment) and aluminum welding wire (to simulate bolt); (2) To carry out the model test with homemade loading device, and analyze the η value of the segmental ring models respectively; and (3) To compare the laboratory model tests results with the previous research and give the recommended η value and value range.

It is worth mentioning that the laboratory structural model testing result about the effective ratio of the longitudinal bending rigidity will be discussed in the companion of this paper.

2. Design of model test

2.1. Similarity relations of the model test

2.1.1. Similarity relations of segment

When segmental structure prototype and model bear corresponding static force, the variables that can be compared in geometry and static effect mainly include:

(1) Geometry size: outer diameter of segmental ling (D), segment thickness (t), and segment ring width (b).
(2) Material properties: segment elastic modulus (E_s), segment unit weight (γ), and segment Poisson ratio (μ).
(3) External load: concentrated force (F), uniform load (q), and bending moment (M).
(4) Stress and deformation parameters: stress in segment (σ), strain of segment (ε), bending of segmental ring (δ), and rotation angle of segment (θ).

The similarity of segment unit weight γ was not considered in this model test, as the dead weight of segmental ring is much less than the overburden pressure and the ground overload. The similarities of the uniform load q and bending moment M were also be neglected since the concentrated force loading was the only external load in the model test. From this we can see that the dimensional parameters in similarity relation include the geometry size S (outer diameter of segmental ling D, segment thickness t, segment ring width b), segment elastic modulus E_s, concentrated force F, stress in segment σ, bending of segmental ring δ. Let α_1, α_2, α_3, α_4, α_5, represent the powers of the those 5 parameters, then, the similar matrix as follows:

	α_1	α_2	α_3	α_4	α_5
	S	E_s	F	σ	δ
L	1	−2	0	−2	1
F	0	1	1	1	0

(1)

Two linear homogeneous equations (Eq. (2)) can be gotten according this similar matrix:

$$\left.\begin{aligned} L:\ \alpha_1 - 2\alpha_2 - 2\alpha_4 + \alpha_5 = 0 \\ F:\ \alpha_2 + \alpha_3 + \alpha_4 = 0 \end{aligned}\right\} \tag{2}$$

Hypothesizing α_3, α_4, α_5 as the known quantities of the three equations, then, Eq. (3) can be gotten.

$$\left.\begin{aligned} \alpha_1 = -2\alpha_3 - \alpha_5 \\ \alpha_2 = -\alpha_3 - \alpha_4 \end{aligned}\right\} \tag{3}$$

The number n of the parameters with dimensions equals 5, and the basic dimension equals 2 (taking the length dimension S and force dimension F as the basic dimensions). According to the π theorem, there are 3 similarity criterions. Consequently, α_3, α_4, α_5 should be given three groups of values, and the simplest way is one of which equals 1 and the remaining values are equal to zero. Therefore, we can get:

When $a_3 = 1$, $a_4 = a_5 = 0$, then, $a_1 = -2$, $a_2 = -1$.
When $a_4 = 1$, $a_3 = a_5 = 0$, then, $a_1 = 0$, $a_2 = -1$.
When $a_5 = 1$, $a_3 = a_4 = 0$, then, $a_1 = -1$, $a_2 = 0$.

According to the similarity law $\pi L^{a1} E_s^{a2} F^{a3} \sigma^{a4} \delta^{a5}$, 3 similarity criterions can be obtained, which is: $\pi_1 = F/(EsL^2)$, $\pi_2 = \sigma/Es$, and $\pi_3 = \delta/L$.

Using subscript "p" and "m" to represent the prototype and model respectively, the similarity constants can be expressed as:

$$C_L = \frac{D_p}{D_m} = \frac{t_p}{t_m} = \frac{b_p}{b_m}, \quad C_{E_s} = \frac{(E_s)_p}{(E_s)_m}, \quad C_\mu = \frac{\mu_p}{\mu_m}, \quad C_\sigma = \frac{\sigma_p}{\sigma_m},$$
$$C_\varepsilon = \frac{\varepsilon_p}{\varepsilon_m}, \quad C_\delta = \frac{\delta_p}{\delta_m}, \quad C_\theta = \frac{\theta_p}{\theta_m}, \quad C_F = \frac{F_p}{F_m}$$

where C denotes the similarity constant between the prototype and the model, while the subscript is the corresponding parameter involved in the system, for instance, C_L is the geometric similarity ratio, and the rest symbols may be deduced by analogy.

With the principle of meeting the geometric and elastic modulus similarity, on the basis of dimensional analysis method, the relations between similarity constants can be deduced as follows:

$$C_\sigma = C_{E_s}, \quad C_\delta = C_L, \quad C_\mu = C_\varepsilon = 1, \quad C_F = C_{E_s} C_L^2.$$

2.1.2. Similarity relations of joint

Since the segmental lining is made up of large number of segments, numerous circumferential and longitudinal joints then formed and which are connected by bolts, the difficulty of shield tunnel model test just lies in the joint similarity. The variables of bolt that can be compared in geometry and static effect mainly include: diameter of the bolt (d), length of the bolt (l) and elastic modulus of the bolt (E_b), among which the diameter d and length l can be derived through the same geometric similarity ratio of the segment, the elastic modulus is ascertained according to the model tunnel with the same bending rigidity ratio and compressive (or extensional) rigidity ratio between the segment and bolt of the prototype tunnel. The specific steps are as follows:

(1) To calculate the bending rigidity ratio and compressive (or extensional) rigidity ratio $(\alpha_{ij})_p$ between the segment and joint bolt of the prototype tunnel (shown in Table 1. Note: $i = 1$ means circumferential joint, $i = 2$ means longitudinal joint; $j = 1$ means bending, $j = 2$ means compressive or extensional).
(2) To select a pair of model material of segment and bolt, and ascertain the geometry size according to geometric similarity ratio to be adopted, which includes segment model's thickness, diameter and width, and bolt model's length and diameter. Then, calculate the bending rigidity ratio and compressive (or extensional) rigidity ratio $(\alpha_{ij})_{m0}$ between the segment model and a single joint model.
(3) To compare the $(\alpha_{ij})_p$ and $(\alpha_{ij})_{m0}$, the bolt number of circumferential and longitudinal direction can be obtained. It is worth mentioning that each model segment must have one corresponding model bolt at least, for ensuring the segmental ring model can be connected smoothly. In other words, the minimal number of the model bolt of circumferential and longitudinal direction is 6, since there are 6 segments in one segmental ring in total in the test model.
(4) To calculate the bending rigidity ratio and compressive (or extensional) rigidity ratio $(\alpha_{ij})_m$ between the segment and joint bolt of the model tunnel, according to their geometry size and elastic modulus.
(5) To calculate the bending and compressive (or extensional) rigidity similarity degree β_{ij} of the joint bolts between the model tunnel and the prototype tunnel by Eq. (4), through comparing the $(\alpha_{ij})_m$ and $(\alpha_{ij})_p$.

$$\beta_{ij} = 1 - \frac{|(\alpha_{ij})_p - (\alpha_{ij})_m|}{(\alpha_{ij})_m} \tag{4}$$

(6) To calculate the rigidity similarity degree of the joint bolts under all model material combinations in accordance with the above steps, and select segment and bolt model combination which has maximal rigidity similarity degree.
(7) To ensure the elastic modulus similarity ratio of the segment and bolt model on the basis of the related parameters of model and prototype material, then, obtain the load similarity ratio under direction of geometric similarity ratio.

The above steps can be expressed by flow chart of Fig. 3.

2.2. Material selection

2.2.1. Tensile test of segment model material

The POM (Polyoxymethylene), ABS (Acrylonitrile butadiene styrene), Nylon materials and PMMA (Polymethylmethacrylate) are preliminarily selected for making the segment model after extensive comparison and screening, as there are many kinds of materials which can be used for the segment model. Then, the tensile elastic modulus can be got by tensile test on the four materials. The obtained stress and strain relationship and material properties through the tensile test is shown in Table 2.

2.2.2. Tensile test on bolt model material

The bolt model material must be adapted for thread producing so that it could meet the requirements of segment assembly, besides reaching the geometric and elastic modulus similarity. We found that the welding wire used in metal welding process maybe meet the requirements of bolt material based on a large number of data accesses and market researches, which are very suitable for secondary operation as a pure metal material for one side, and has the special characteristics of small geometry size, fine workmanship and low price for the other side. Therefore, under the condition of satisfying the geometric similarity, three kinds of welding wire, including aluminum wire (type HS301), iron wire (type J50) and steel wire (type ER325), were selected to make specimen and carry out the tensile test. The result of the tensile test is shown in Table 2.

2.2.3. Combination analysis on the model material

Now, we let the aforementioned preliminarily selected four segment materials and three bolt materials combine with each other, and substitute the elastic modulus concluded from tensile tests

Table 1
Rigidity ratio between segment and joint of model tunnel and prototype tunnel.

(α_{ij})	Prototype (p)		Model (m)	
	Bending ($j = 1$)	Compressive and extensional ($j = 2$)	Bending ($j = 1$)	Compressive and extensional ($j = 2$)
Transverse joints ($i = 1$)	$\frac{(E_s I_{hs})_p}{(n_h E_b I_{hb})_p}$	$\frac{(E_s A_{hs})_p}{(n_h E_b A_b)_p}$	$\frac{(E_s I_{hs})_m}{(n'_h E_b I_{hb})_m}$	$\frac{(E_s A_{hs})_m}{(n'_h E_b A_b)_m}$
Longitudinal joints ($i = 2$)	$\frac{(E_s I_{vs})_p}{(n_v E_b I_{vb})_p}$	$\frac{(E_s A_{vs})_p}{(n_v E_b A_b)_p}$	$\frac{(E_s I_{vs})_m}{(n'_v E_b I_{vb})_m}$	$\frac{(E_s A_{vs})_m}{(n'_v E_b A_b)_m}$

where: $I_{hs} = bt^3/12$, $I_{hb} = \pi d^4/64$, $A_{hs} = bt$, $I_{vs} = \frac{\pi}{64}[D^4 - (D-2t)^4]$, $I_{vb} = \pi d^4/64$, $A_{vs} = \frac{\pi}{4}[D^2 - (D-2t)^2]$, $A_b = \pi d^2/4$, n_h is the transverse bolt number of the prototype tunnel, n'_h is the transverse bolt number of the model tunnel, n_v is the longitudinal bolt number of the prototype tunnel, n'_v is the longitudinal bolt number of the model tunnel.

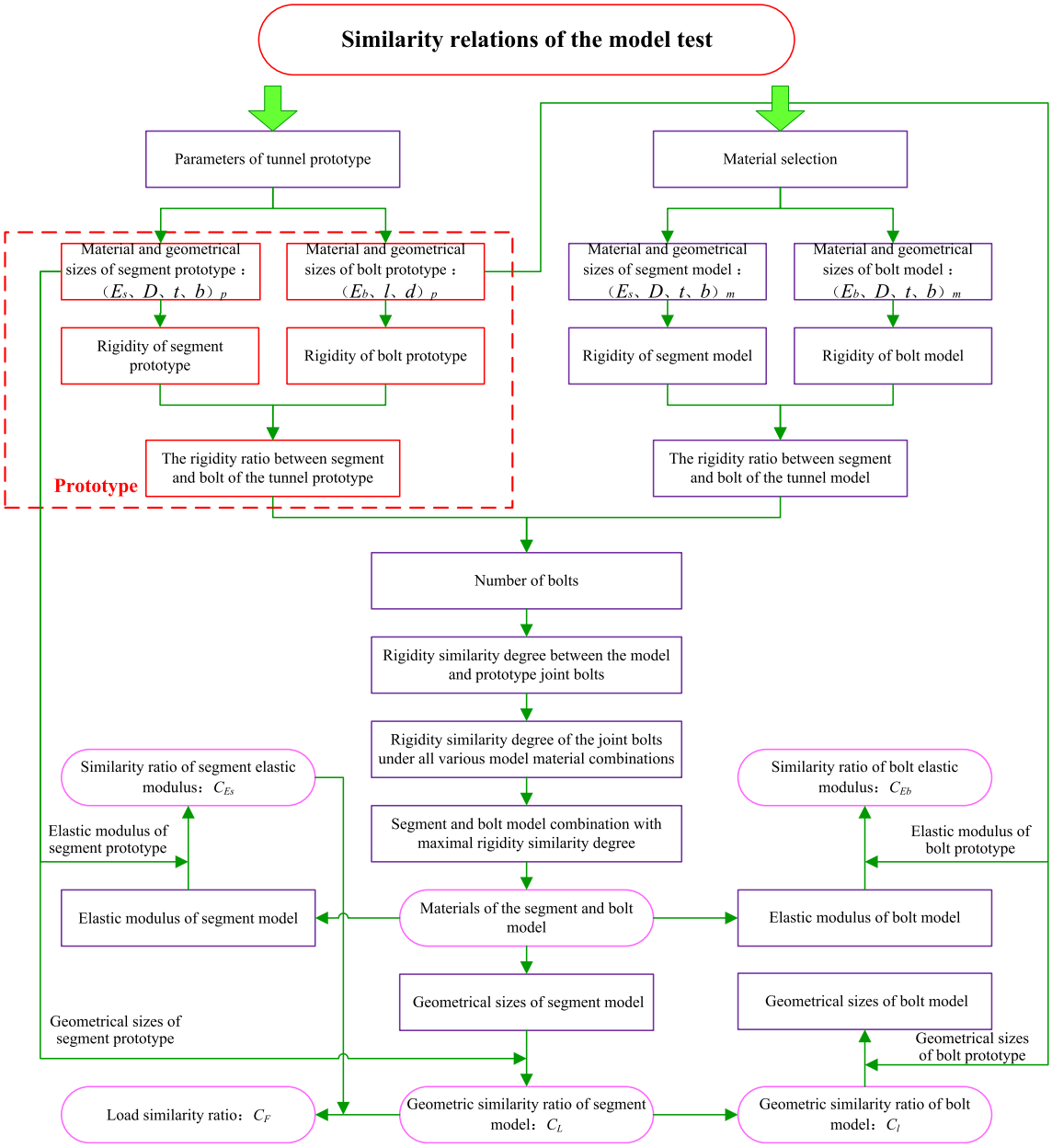

Fig. 3. The flow chart of ensuring the similarity ratio of the model tunnel.

Table 2
Tensile test results of the preselected segment material.

Types	Tensile strength (MPa)	Fracture stress (MPa)	Elastic modulus (MPa)
Polyoxymethylene	31.32	26.67	1386
Acrylonitrile butadiene styrene	60.61	55.79	1780
Nylon	40.51	39.87	612.6
Polymethylmethacrylate	53.33	52.64	2091
Aluminum welding wire	218.5	177.4	33,800
Iron welding wire	888.9	528.3	74,300
Steel welding wire	881.4	634.8	87,630

and other parameters into Table 1 and Eq. (4), then, obtain the rigidity similarity degree of the joint bolts between the model tunnel and the prototype tunnel (shown in Table 3). From Table 3 we can see that the rigidity similarity degree between the combination of PMMA and aluminum welding wire and the prototype is the maximum, the average value of which reaches 0.815. Certainly, it is the best status if the rigidity similarity degree between the model and the prototype value is 1, but this kind of material combination is almost impossible to be found as it is limited by the elastic modulus and divergence of bolt amount. So, the finally selected model material is PMMA (to simulate segment) and aluminum welding wire (type HS301, to simulate bolt). The mechan-

Table 3
The rigidity similarity degree of the joint bolts between the model tunnel and the prototype tunnel.

Similarity degree		Polyoxymethylene		Acrylonitrile butadiene styrene		Nylon		Polymethylmethacrylate	
		Bending	Compressive and extensional	Bending	Compressive and extensional	Bending	Compressive and extensional	Bending	Compressive and extensional
Aluminum	Transverse	0.48	0.50	0.62	0.64	0.21	0.22	0.71	0.74
	Longitudinal	0.59	0.63	0.76	0.81	0.26	0.28	0.88	0.93
Iron	Transverse	0.22	0.23	0.28	0.29	0.10	0.10	0.33	0.33
	Longitudinal	0.27	0.29	0.34	0.37	0.12	0.13	0.40	0.43
Steel	Transverse	0.19	0.19	0.24	0.25	0.08	0.08	0.28	0.28
	Longitudinal	0.23	0.24	0.29	0.31	0.10	0.11	0.34	0.36

ical and geometric properties of model and prototype tunnel, and the similarity ratio of the model tests can be found in Table 4–6 respectively.

2.3. Model design and fabrication

2.3.1. Model design

The simulation prototype object of this model test is the universal subway tunnel in China, which usually use the C50 type RC segment and HRB335 type steel bolt by straight-jointed or stagger-jointed assembly. It would not achieve the assembly because of its small size, if the model tunnel was designed in full accordance with the prototype tunnel. Therefore, some adjustment was adopted in the model design under the pre-condition of not affecting the structure stress and deformation:

(1) Although the curved bolts are often used in practical segments, the sizes of model bolts are too small to bend. So, the straight bolts are adopted in the model test.
(2) Usually, the hand holes are located inside of the segments in real case. For the convenience of assembling bolt, the hand holes are moved from segment inside to outside under the pre-condition of not changing the bolts location.
(3) On the corresponding position of segment outside surface, some slots are chiseled for providing the operational space in facilitating to install bolts and nuts, in fact, that are not exist in practical shield tunnel engineering.
(4) Straight edge is adopted in model segment, although the key segment and adjacent segments of the prototype tunnel segments usually are bevel edge.

Besides the above mentioned differences between the model and the prototype, watertight strips at the joints are omitted in the model tunnel, and the pre-tightening forces of joint bolts are not completely consistent with the real case as well. Figs. 4 and 5 show the structure and the distribution of the longitudinal and circumferential bolts of the model segmental ring respectively, Fig. 6 shows the hand holes distribution of the prototype and model tunnel, and Fig. 7 is the effect drawing of the segmental ring model.

2.3.2. Model fabrication

The model fabrication process includes three main steps: segment and bolt manufacturing, and segment assembly. The specific flow chart of the model fabrication is shown in Fig. 8.

(1) Segment fabrication.

A complete PMMA pipe with 2000 mm in length, 400 mm in outside diameter and 23 mm in thickness is used to fabricate the segment model according to the design specifications. Two main steps are involved in the fabricating process. They are transverse cutting and polishing, and longitudinal cutting and polishing. The first step, transverse cutting, means that the PMMA pipe with

Table 4
The mechanical properties of model and prototype tunnel.

Types	Elastic modulus of segment (Pa)	Poisson's ratio of segment	Elastic modulus of joint (Pa)	Poisson's ratio of joint
Prototype	3.45E+10	0.2	2.00E+11	0.3
Model	2.06E+09	0.3	3.38E+10	0.32

Table 5
The geometric properties of model and prototype tunnel.

Types	Lining outside diameter (m)	Lining outside diameter (m)	Lining thickness (m)	Ring width (m)	Length of bolt (m)	Diameter of bolt (m)	Transverse bolts number	Longitudinal bolts number
Prototype	6.2	5.5	0.35	1	0.4	0.03	13	17
Model	0.4	0.355	0.023	0.065	0.027	0.002	6	6

Table 6
Similarity ratio of model tests.

Types	Geometric similarity ratio	Elastic modulus similarity ratio	Load similarity ratio
Segment model	15.5	16.72	4015.81
Bolt model	15	5.92	

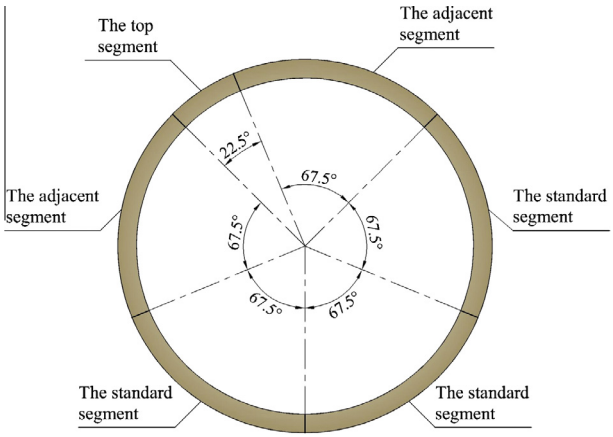

Fig. 4. The segment partition scheme.

2000 mm in length is divided into single rings with a segment width. The second step, longitudinal cutting, is to cut the single ring that just got from the first step into separate segments according to the segment partition scheme shown in Fig. 4. Polishing is to tread on the heels of the last two steps, the purpose of which is to make the model fine and strictly comply with the design requirements as far as possible.

Next, we need to punch holes and chisel slots, the concrete steps of which include: marking, punching and slotting. Marking is to mark a position for the hole or slot on the segment surface under the help of a pre-produced mold. Punching is to drill the longitudinal and circumferential holes with bench drilling machine. Slotting is to chisel slot on the corresponding position of segment outside surface for providing the operational space in facilitating installing bolt and nut.

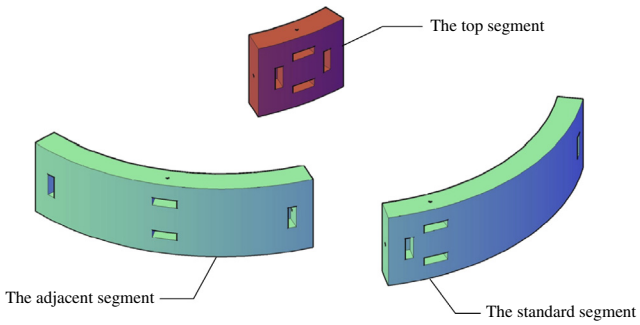

Fig. 6. The hand holes distribution of the segment model.

(2) Bolt fabrication.

The precision screw die tool is used to make bolt by hands, as the diameter of the bolt model is only 2 mm. Firstly, cut the aluminum welding wire (type HS301) into rods in accordance with the design length, and strictly control the length by end grinding. Then, make screw at two ends of the bolt with the 2 mm screw die tool. The nuts and spring gaskets corresponding to the bolt model with 2 mm in diameter can be easily bought in market and need not be made by hands.

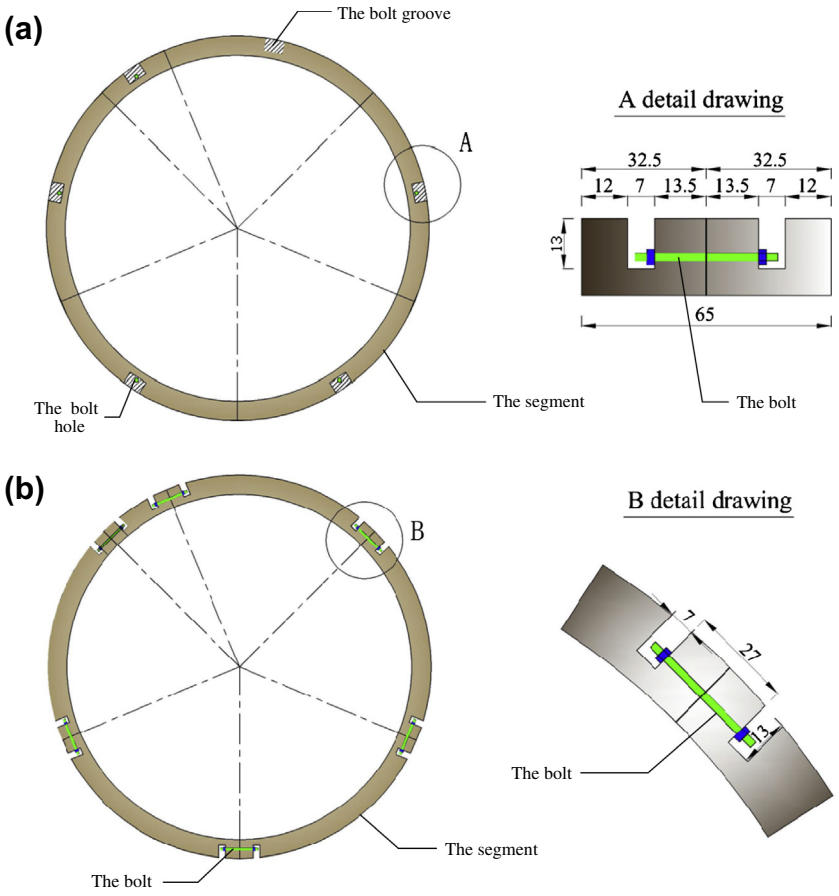

Fig. 5. (a) The longitudinal bolts distribution (unit: mm). (b) The circumferential bolts distribution (unit: mm).

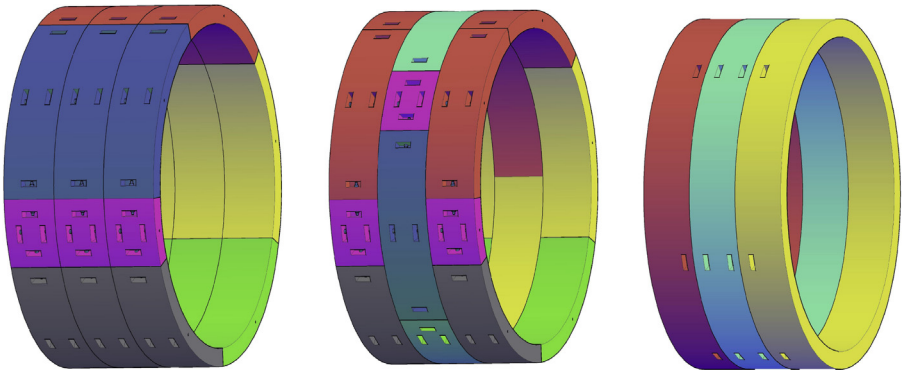

The effect drawing of the straight –jointed segmental ring model

The effect drawing of the stagger –jointed segmental ring model

The effect drawing of the uniform segmental ring model

Fig. 7. The ring model.

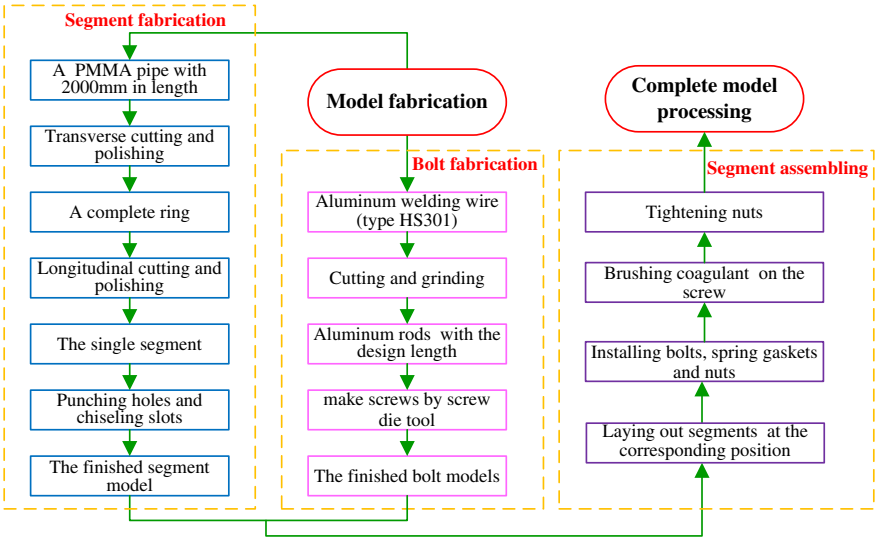

Fig. 8. The flow chart of the model fabrication.

(3) Model assembly.

The segment and bolt models then can be assembled with straight-jointed, stagger-jointed and uniform ring, which are in accordance with Fig. 7. According to the segment partition scheme shown in Fig. 4, the segments are laid out at the corresponding position one by one, the bolts, spring gaskets and nuts then are assembled in turn. After that, the coagulant is brushed on the screw for increasing bite force between the bolt and nut. At last, the assembly process is finished after tightening nut.

2.4. Test devices and method

2.4.1. Test devices

The model test is a static loading test based on the load structure method.

2.4.2. Load system

The segmental ring model was loaded at vault position using a square box, some iron sands, a piece of iron plate and some weights. There are nine steps loading in total in the test and each load value is 2 kg. The specific loading steps are as follows:

(1) The square box, called loading box in this paper, was pasted on the vault.
(2) Applying the first load through putting the iron sands and iron plate into the loading box (the total weight is 2 kg), which then avoids the influence of the arc surface and provides a platform for the next loading.
(3) Applying the second load by adding four weights, the total weight of which is 2 kg.
(4) Repeat the third step until nine stages loading completed.

2.4.3. Data acquisition system

The static data collecting gauge type DH3816 and mechanical and electric resistance strain displacement sensor type WBD are used to measure and collect the displacement rates of representative positions of the segmental ring model. There are interrelations between adjacent segmental rings as many segmental rings bearing load together in the practical engineering. So, three segmental rings model are used in the test and attention focus on mechanical properties of the middle ring. The measurement contents mainly refer to radial displacements of the representative points of the middle ring, which are equidistantly distributed on the position with every 45° angle from vault. There are seven radial displacements sensors in total along the circumference in the test, shown in Fig. 9.

2.4.4. Design of test content

The model test purpose in this paper is to study the transverse bending rigidity efficiency, and the transverse performance

comparison of the segmental ring under different bolt pre-tightening forces.

There are 4 groups of experiments in the test (shown in Table 7). The first group is for studying the stress and deformation of the transverse uniform ring, which is the simplified analyzing model of the average uniform rigidity ring method. The second and third group is for studying the stress and deformation of the straight-jointed and stagger-jointed segmental ring, in which one spring gasket and two nuts are installed at every bolt's ends. However, instable failure phenomenon appeared in the loading process of model TFGPMX-02 resulted from the insufficient bolt pre-tightening forces. So, some adjustment and improvement in changing one spring gasket and two nuts into two spring gaskets and two nuts and paste is adopted in the fourth group, for solving the pre-tightening forces deficiency problem.

3. Model test results and discussion

3.1. The transverse deformation characteristic

Fig. 10 shows the deformation results of the middle ring under group 1 and 4 test conditions after loading, from which, we can see that:

(1) The deformation characteristics of the three kinds of segmental ring model are basically the same, in detail, the deformation value of the vault is the largest, horizontal diameter position is the second, and the four points at 45°, 135°, 225° and 315° angle are relatively small.

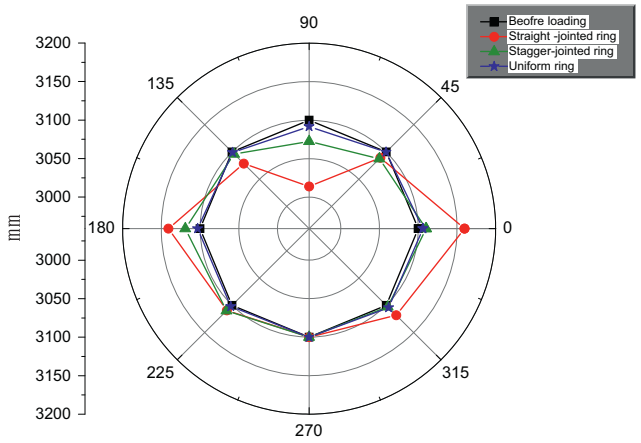

Fig. 10. The deformation results of the middle ring.

(2) Under the same loading condition, straight-jointed segmental ring has the largest deformation rate, followed by the stagger-jointed ring, and the uniform ring is the minimal.

And then, we can conclude that:

(1) Compared with uniform ring, the transverse bending rigidity significantly reduced because of the longitudinal joints. So, in the uniform rigidity ring model, the assumption of the circumferential joint having the same rigidity with that of the segment exits obvious deficiencies: the moment of joint is overestimated and that occurring at the segment is not calculated correctly.

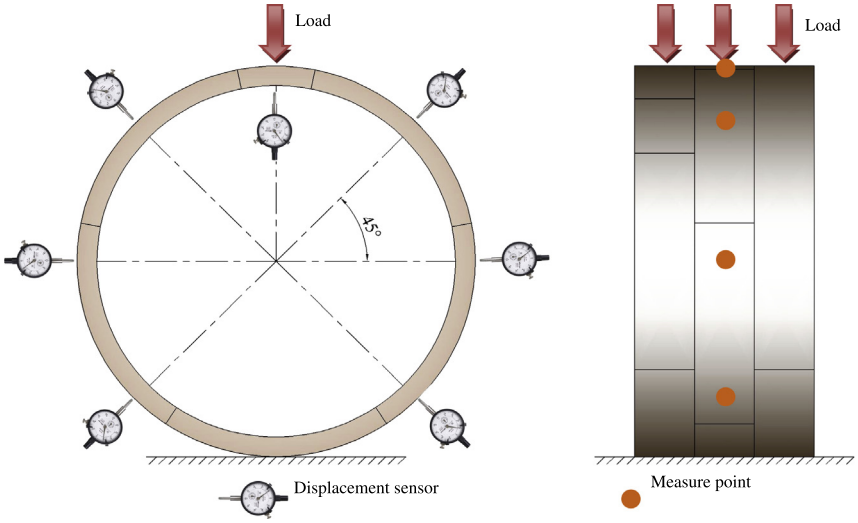

Fig. 9. Arrangement of measurement points.

Table 7
Test conditions.

Groups	Test model number	Assembling method	Longitudinal and transverse connection method
1	YZGPMX-01	Three uniform ring	Uniform in transverse direction and bolts connected in longitudinal direction
2	TFGPMX-01 CFGPMX-02	Three straight-jointed rings Three stagger-jointed rings	Aluminum bolts + one spring gasket + two nuts
3	TFGPMX-02 CFGPMX-03	Three straight-jointed rings Three stagger-jointed rings	Aluminum bolts + one spring gasket + two nuts
4	TFGPMX-06 CFGPMX-07	Three straight-jointed rings Three stagger-jointed rings	Aluminum bolts + one spring gasket + two nuts + paste

(2) The transverse deformation value of the stagger-jointed segmental ring is smaller than that of the straight-jointed ring, as the longitudinal joints of stagger-jointed segmental ring, affected by adjacent segments, bear a smaller moment than that of the main cross section.

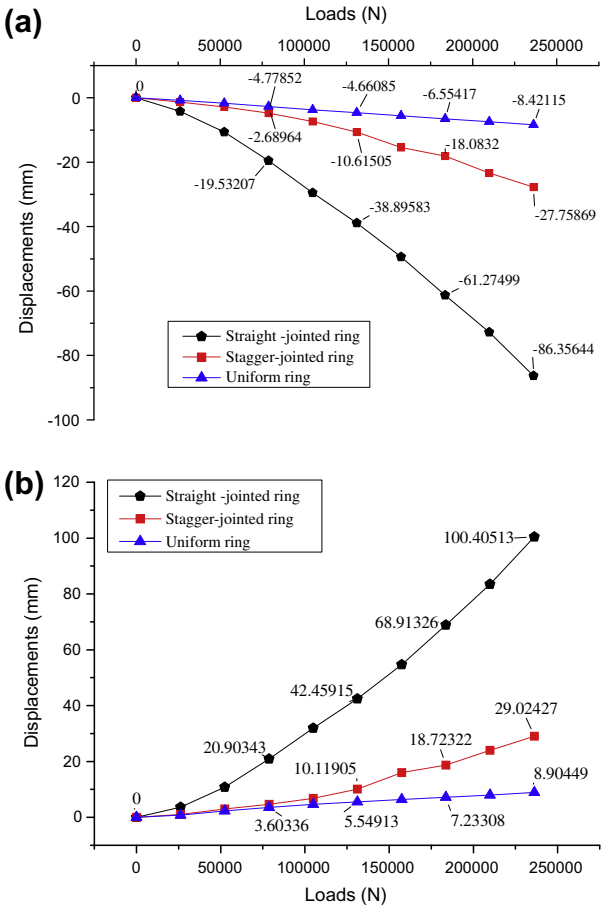

Fig. 11. (a) The vertical diameter variation curves of the middle ring with the increase of the load. (b) The horizontal diameter variation curves of the middle ring with the increase of the load.

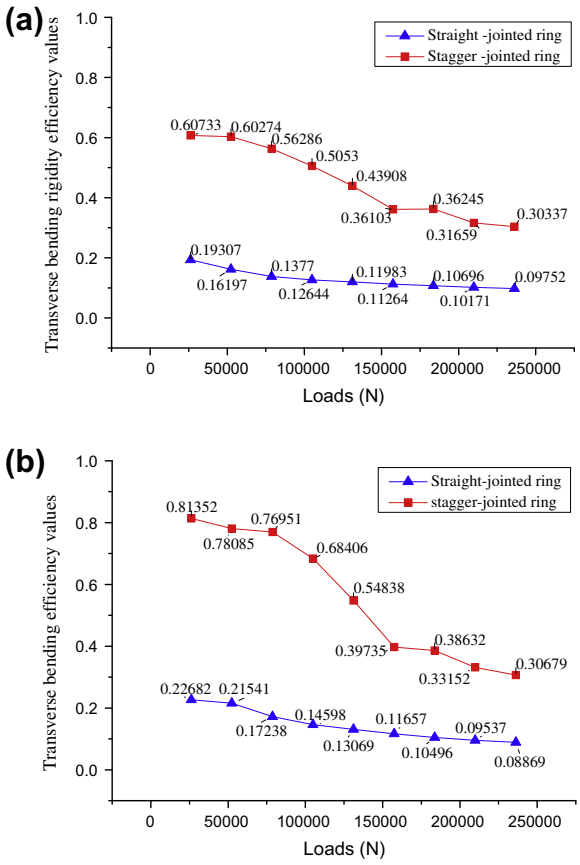

Fig. 13. (a) The relationship between transverse bending efficiency values and loads (base on vertical diameter variation). (b) The relationship between transverse bending rigidities and loads (base on horizontal diameter variation).

In fact, the above two points just illustrate the rationality of the effective ratio of the transverse bending rigidity η and the additional rate of bending moment ξ in average uniform rigidity ring method.

Fig. 11 shows the vertical and horizontal diameter variation curves of the middle ring with the increase of the load under group 1 and 4 test conditions, from which, we can see that:

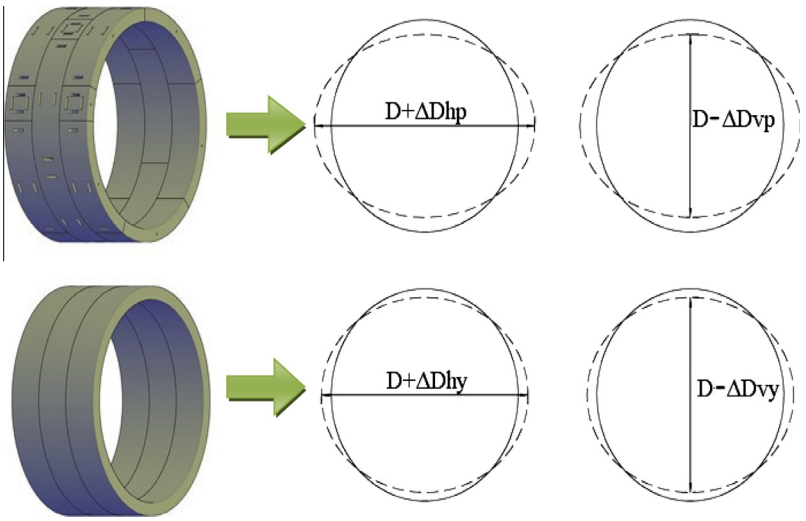

Fig. 12. Calculation diagram of transverse bending rigidity efficiency.

(1) With the increase of the load, the horizontal and vertical diameter shows a linear increase and linear decrease respectively in the whole loading process.
(2) The deformation characteristics of the horizontal and vertical diameter under conditions of stagger-jointed ring, straight-jointed ring and uniform ring are basically the same. The major difference lies in the slope of the three curves, which also illustrates the difference of transverse bending rigidity of the three kind of segmental ring models.

3.2. The transverse bending rigidity calculation

According to research findings of Huang et al. (2006a,b), the slope ratio of load vs. displacement curve of all kinds of segmental ring is just the inverse ratio of the corresponding transverse bending rigidity, which illustrates that the variation value of horizontal or vertical diameter of different segmental rings under the same load change condition reflects the bending rigidity of the segmental ring (shown in Fig. 12). Accordingly, in this paper, the transverse bending rigidity efficiency is defined as:

$$\begin{cases} \eta_1 = \Delta D_{hy}/\Delta D_{hp} \\ \eta_2 = \Delta D_{vy}/\Delta D_{vp} \end{cases} \quad (5)$$

where ΔD_{hp} is the horizontal diameter variation value of the assembled segmental ring (including straight-jointed and stagger-jointed ring); ΔD_{hy} is horizontal diameter variation value of the uniform segmental ring; ΔD_{vp} is the vertical diameter variation value of the assembled segmental ring (including straight-jointed and stagger-jointed ring); and ΔD_{vy} is vertical diameter variation value of the uniform segmental ring.

According to Eq. (5), the transverse bending rigidities of straight-jointed and stagger-jointed ring under each load level can be calculated, the relationship between which and loads can be described by curves shown in Fig. 13, and the value range of which are shown in Table 8.

It is found from Fig. 13 and Table 8 that the transverse bending rigidity efficiency value calculated by horizontal diameter is slightly larger than that by vertical diameter. In fact, the actual transverse bending rigidity efficiency value of the segmental ring in practical engineering should be larger than that of the model test, because of the influence of the surrounding soil. So, this paper suggests that the transverse bending rigidity efficiency value is subject to the horizontal diameter variation value, the calculated range of which is between 0.09 and 0.23 under straight-jointed condition, 0.30 and 0.80 under stagger-jointed condition.

Table 8
The transverse bending rigidity efficiency value from test.

Types	Calculated by vertical diameter variations	Calculated by horizontal diameter variations
Straight-jointed	0.10–0.19	0.09–0.23
Stagger-jointed	0.30–0.61	0.30–0.80

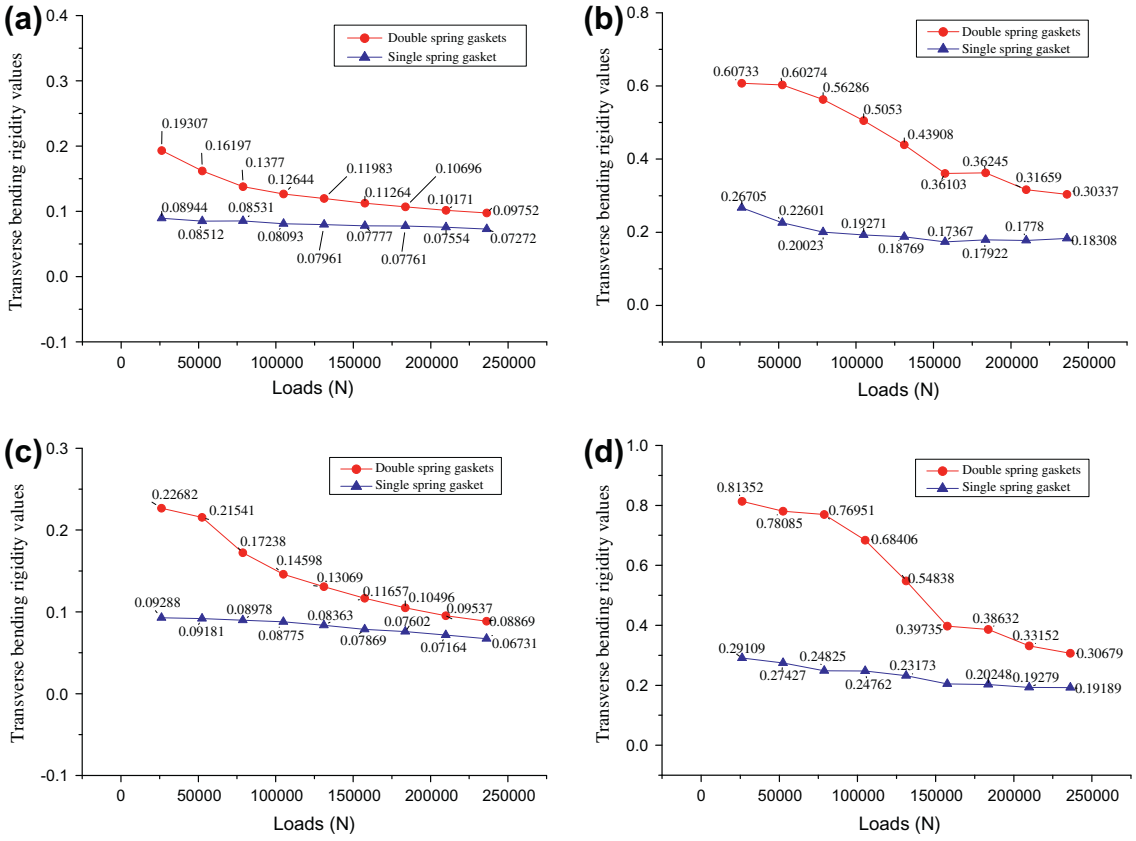

Fig. 14. (a) The relationship between the effective ratios of the transverse bending rigidity of straight-jointed and loads under the different spring gasket numbers (base on vertical diameter variation). (b) The relationship between the effective ratios of the transverse bending rigidity of stagger-jointed and loads under the different spring gasket numbers (base on vertical diameter variation). (c) The relationship between the effective ratios of the transverse bending rigidity of straight-jointed and loads under the different spring gasket numbers (base on horizontal diameter variation). (d) The relationship between the effective ratios of the transverse bending rigidity of stagger-jointed and loads under the different spring gasket numbers (base on horizontal diameter variation).

3.3. Influence of bolt pre-tightening forces on the transverse bending rigidity

The bolts in the test are made of aluminum welding wire (type HS301) by hands, the pre-tightening forces of which is realized by mechanical bite force between the thread and nut, and the pressure between spring gasket and nut. So, the different bolt pre-tightening forces can be obtained by different number of spring gaskets. The spring gaskets numbers in the four groups of experiments in the test are listed in Table 7. The bolt size is so small that we cannot measure the pre-tightening force of which conveniently. So, in this paper, we qualitatively evaluate the influence of bolt pre-tightening forces on the transverse bending rigidity just through changing the spring gasket number.

Fig. 14 shows the relationship between the effective ratios of the transverse bending rigidity of straight-jointed and stagger-jointed ring and loads under the different spring gasket numbers, from which we can see that:

(1) The effective ratio of the transverse bending rigidity of the segmental ring decreases with the load increasing under single spring gasket and double spring gaskets conditions, and the former decreases faster.
(2) Under same loading condition, the effective ratio of the transverse bending rigidity value of the segmental ring with double spring gaskets is obviously lager than that under single spring gasket condition. This indicates that increasing bolt pre-tightening force is favorable for improving the effective ratio of the transverse bending rigidity value.
(3) With the load increasing, the effective ratio of the transverse bending rigidity value difference between single and double spring gaskets decrease gradually.

4. Conclusions

Based on model test on the straight-jointed ring, stagger-jointed ring and uniform ring, the following conclusions can be drawn:

(1) With the principle of the same joint rigidity ratio between the model and the prototype tunnel, the PMMA and aluminum welding wire are used to simulate the segment and bolt separately. The similarity relation at the joint area is achieved through the model tunnel having the same rigidity ratios with the prototype tunnel. This experimental method is proved to be feasible to carry out segmental structure model test.
(2) The deformation characteristics of straight-jointed ring, stagger-jointed ring and uniform ring are basically the same, which shows a linear changing with the increase of the load. The major difference lies in the slope of the three loads–deformation curves, which resulted from the difference of transverse bending rigidity of the three kind of segmental ring models.
(3) The test results show that the range of the effective ratio of the transverse bending rigidity value is between 0.09 and 0.23 under straight-jointed condition, 0.30 and 0.80 under stagger-jointed condition.
(4) The effective ratio of the transverse bending rigidity value of the segmental ring decreases with the load increasing under straight-jointed and stagger-jointed conditions, and the latter decreases faster. Under the same loading condition, the effective ratio of the transverse bending rigidity of the stagger-jointed segmental ring is obviously lager than that of the straight-jointed segmental ring, and that difference decrease gradually with the load increasing.

Acknowledgements

This study was supported by the National Natural Science Foundation of China (Grant Nos. 51178052 and 50808020) and the Fundamental Research Funds for the Central Universities (Grant No. CHD2011JC099).

References

Bakker, K.J., 2003. Structural design of linings for bored tunnels in soft ground. Heron 48 (1), 33–63.
British Tunnelling Society, 2004. Tunnel Lining Design Guide. Thomas Telford, London.
DAUB, 2001. Concrete linings for tunnel built by underground construction. Tunnel 5, 50–66.
Ding, W.Q., Yue, Z.Q., Tham, L.G., Zhu, H.H., Lee, C.F., Hashimoto, T., 2004. Analysis of shield tunnel. Int. J. Numer. Anal. Meth. Geomech. 28, 57–91.
Duddeck, H., Erdmann, J., 1982. Structural design models for tunnels. In: Tunnelling 82, Proceedings of the 3rd International Symposium, Brighton, 7–11 June, 1982, pp. 83–91.
Feng, K., He, C., Xia, S.L., 2011. Prototype tests on effective bending rigidity ratios of segmental lining structure for shield tunnel with large cross-section. Chin. J. Geotech. Eng. 33 (11), 1750–1758 (in Chinese).
Gruebl, F., 2006. Modern design aspects of segmental lining. In: International Seminar on Tunnels and Underground Works, LNEC, Lisbon, 29–30 June, 2006.
Grübl, F., Thewes, M., 2006. Recommendations of the German working group on design and calculation of shield machines. Tunn. Undergr. Sp. Technol. 21 (3), 261–266.
Gruebl, F., 2012. Segmental ring design – new challenges with high tunnel diameters. In: Proceedings of the World Tunnel Congress 2012, Bangkok, Thailand. pp. 2–11.
Hu, X.Y., Zhang, Z.X., Teng, L., 2009. An analytical method for internal forces in DOT shield-driven tunnel. Tunn. Undergr. Sp. Technol. 24, 675–688.
Huang, H.W., Xu, L., Yan, J.L., Yu, Z.K., 2006a. Study on transverse effective rigidity ratio of shield tunnels. Chin. J. Geotech. Eng. 28 (1), 11–18 (in Chinese).
Huang, X., Huang, H.W., Zhang, J., 2012. Flattening of jointed shield-driven tunnel induced by longitudinal differential settlements. Tunn. Undergr. Sp. Technol. 31, 20–32.
Huang, Z.H., Ji, Q.Q., Lin, J.X., 2010. Experimental study on the anti-uplift of super-large diameter slurry balance shield tunnel structure. Chin. J. Undergr. Sp. Eng. 6 (2), 250–254 (in Chinese).
Huang, Z.R., Zhu, W., Liang, J.H., 2006b. Study on effective bending rigidity ratios and moment increasing rates in modified routine method. Ind. Const. 36 (2), 45–49 (in Chinese).
Hudoba, I., 1997. Contribution to static analysis of load-bearing concrete tunnel lining built by shield-driven technology. Tunn. Undergr. Sp. Technol. 12 (1), 55–58.
I.T.A. Working Group No. 2. (ITA), 2000. Guidelines for the design of shield tunnel lining. Tunn. Undergr. Sp. Technol. 15, 303–331.
Japan Society of Civil Engineers, 1977. The Design and Construction of Underground Structures, Tokyo (in Japanese).
Japan Society of Civil Engineers, Zhu, W. translates, 2001. Japanese Standard for Shield Tunneling. China Construction Industry Press, Beijing, China (in Chinese).
Kashima, Y., Kondo, N., Inoue, M., 1996. Development and application of DPLEX shield method: results of experiments using shield and segment models and application of the method in tunnel construction. Tunn. Undergr. Sp. Technol. 41, 45–50.
Kasper, T., Meschke, G., 2004. A 3D finite element simulation model for TBM tunnelling in soft ground. Int. J. Numer. Anal. Meth. Geomech. 28, 1441–1460.
Kasper, T., Meschke, G., 2006. On the influence of face pressure, grouting pressure and TBM design in soft ground tunnelling. Tunn. Undergr. Sp. Technol. 21, 160–171.
Klappers, C., Grübl, F., Ostermeier, B., 2006. Structural analyses of segmental lining – coupled beam and spring analyses versus 3D-FEM calculations with shell elements. In: Proceedings of the ITA-AITES 2006 World Tunnel Congress, Safety in the Underground Space, 6pp.
Koyama, Y., Nishimura, T., 1998. The design of lining segment of shield tunnel using a beam-spring model. Quart. Rep. RTRI 39 (1), 23–27.
Koyama, Y., 2000. Study on the improvement of design method of segments for shield-driven tunnels. RTRI Report: Special No. 33, RTRI, p. 114 (in Japanese).
Koyama, Y., 2003. Present status and technology of shield tunnelling method in Japan. Tunn. Undergr. Sp. Technol. 18, 145–159.
Lee, K.M., Hou, X.Y., Ge, X.W., Tang, Y., 2001. An analytical solution for a jointed shield-driven tunnel lining. Int. J. Numer. Anal. Meth. Geomech. 25, 365–390.
Lee, K.M., Ge, X.W., 2001. The equivalence of a jointed shield-driven tunnel lining to a continuous ring structure. J. Can. Geotech. Eng. 38, 461–483.
Liao, S.M., 2002. Research on the mechanism of longitudinal shear transfer of circular tunnel. D. Phil. Thesis, Tongji University, Shanghai, China (in Chinese).
Liao, S.M., Peng, F.L., Shen, S.L., 2008. Analysis of shearing effect on tunnel induced by load transfer along longitudinal direction. Tunn. Undergr. Sp. Technol. 23, 421–430.
Liu, J.H., Hou, X.Y., 1991. Shield-Driven Tunnels. China Railway Press, Beijing, China (in Chinese).

Muir Wood, A.M., 1975. The circular tunnel in elastic ground. Geotechnique 25, 115–127.
Peck, R.B., Hendron, A.J., Mohraz, B., 1972. State of the art of soft ground tunnelling. In: Proceedings of the 1st Rapid Excavation and Tunnel Conference, Illinois, vol. 1, pp. 259–286.
Tang, Y., 1988. The mechanism study of the staggering assembly of shield-driven tunnel. M. Phil. Thesis, Tongji University, Shanghai, China (in Chinese).
Uchida, K., 1992. Design and engineering of large bore slurry shield tunnel lining system for Trans-Tokyo Bay Highway. Civ. Eng. Jpn. 30, 54–67.
Xu, L., 2005. Study on the longitudinal settlement of shield tunnel in soft soil. D. Phil. Thesis, Tongji University, Shanghai, China (in Chinese).
Zhong, X.C., Zhu, W., Ji, Y.P., Xu, Y., 2003. The method to confirm the effective bending stiffness of shield-driven tunnel lining. Geol. Prospect. 39 (Suppl. 2), 185–189 (in Chinese).
Zhu, H.H., Tao, L.B., 1998. Study on two beam-spring models for the numerical analysis of segments in shield tunnel. Rock Soil Mech. 19 (2), 26–32 (in Chinese).